SF1-Specific AMPKα1 Deletion Protects Against Diet-Induced Obesity

Patricia Seoane-Collazo,[1,2] Juan Roa,[2,3] Eva Rial-Pensado,[1,2] Laura Liñares-Pose,[1,2] Daniel Beiroa,[1,2] Francisco Ruíz-Pino,[2,3] Tania López-González,[1,2] Donald A. Morgan,[4] José Ángel Pardavila,[1] María Jesús Sánchez-Tapia,[2,3] Noelia Martínez-Sánchez,[1,2] Cristina Contreras,[1,2] Miguel Fidalgo,[1] Carlos Diéguez,[1,2] Roberto Coppari,[5,6] Kamal Rahmouni,[4,7] Rubén Nogueiras,[1,2] Manuel Tena-Sempere,[2,3,8] and Miguel López[1,2]

Diabetes 2018;67:2213–2226 | https://doi.org/10.2337/db17-1538

AMPK is a cellular gauge that is activated under conditions of low energy, increasing energy production and reducing energy waste. Current evidence links hypothalamic AMPK with the central regulation of energy balance. However, it is unclear whether targeting hypothalamic AMPK has beneficial effects in obesity. Here, we show that genetic inhibition of AMPK in the ventromedial nucleus of the hypothalamus (VMH) protects against high-fat diet (HFD)–induced obesity by increasing brown adipose tissue (BAT) thermogenesis and subsequently energy expenditure. Notably, this effect depends upon the AMPKα1 isoform in steroidogenic factor 1 (SF1) neurons of the VMH, since mice bearing selective ablation of AMPKα1 in SF1 neurons display resistance to diet-induced obesity, increased BAT thermogenesis, browning of white adipose tissue, and improved glucose and lipid homeostasis. Overall, our findings point to hypothalamic AMPK in specific neuronal populations as a potential druggable target for the treatment of obesity and associated metabolic disorders.

AMPK is a serine/threonine kinase that is highly conserved throughout evolution. AMPK is a heterotrimer complex comprising a catalytic α subunit (α1 or α2), with a conventional serine/threonine protein kinase domain, and two regulatory subunits, β (β1 or β2) and γ (γ1, γ2, or γ3) (1–3). AMPK is activated by phosphorylation of the α subunit on Thr172, which can be allosterically induced by AMP and catalyzed by several upstream kinases such as liver kinase B1 (LKB1) and calmodulin-dependent kinase kinases, especially CaMKKβ (1–3). Consequently, by detecting changes in the ratio of adenine nucleotides, AMPK is activated by stresses that deplete cellular energy status. By turning off ATP-consuming processes while turning on catabolic processes, AMPK mediates a global counterregulatory response (1–3) that maintains cellular energy homeostasis.

Hypothalamic AMPK plays a major role in the regulation of food intake and energy expenditure (EE), as well as glucose and lipid homeostasis at the whole-body level (4–10). These differential effects of AMPK seem to have an anatomical basis. Whereas the regulatory effects of AMPK on food intake emanate from the arcuate nucleus of the hypothalamus (ARC) (4,6,11,12), its effect on EE stems from the ventromedial nucleus of the hypothalamus (VMH), where AMPK affects the sympathetic nervous system (SNS) to regulate brown adipose tissue (BAT)

[1]Department of Physiology, CiMUS, University of Santiago de Compostela-Instituto de Investigación Sanitaria, Santiago de Compostela, Spain
[2]CIBER Fisiopatología de la Obesidad y Nutrición (CIBERobn), Santiago de Compostela, Spain
[3]Department of Cell Biology, Physiology and Immunology, University of Córdoba, Instituto Maimónides de Investigación Biomédica (IMIBIC)/Hospital Universitario Reina Sofía, Córdoba, Spain
[4]Department of Pharmacology, University of Iowa, Iowa City, IA
[5]Department of Cell Physiology and Metabolism, Faculty of Medicine, University of Geneva, Geneva, Switzerland
[6]Diabetes Center of the Faculty of Medicine, University of Geneva, Geneva, Switzerland
[7]Department of Internal Medicine, University of Iowa, Iowa City, IA
[8]FiDiPro Program, Institute of Biomedicine, University of Turku, Turku, Finland
Corresponding author: Miguel López, m.lopez@usc.es.

Received 17 December 2017 and accepted 27 July 2018.
This article contains Supplementary Data online at http://diabetes.diabetesjournals.org/lookup/suppl/doi:10.2337/db17-1538/-/DC1.
E.R.-P. and L.L.-P. contributed equally to this work.

thermogenesis (7,10,11,13–16). The fact that hypothalamic AMPK controls both feeding and EE, as well as leptin resistance (17,18), makes it an interesting candidate for the treatment of obesity (9,19,20). The aim of this study is to investigate the VMH targeting of AMPK in diet-induced obese (DIO) models. Our data show that ablation of AMPKα1 in steroidogenic factor 1 (SF1) neurons of the VMH protects against high-fat diet (HFD)–induced obesity and that this effect is mediated by increased SNS-driven BAT thermogenesis and browning of white adipose tissue (WAT).

RESEARCH DESIGN AND METHODS

Animals

Adult male Sprague-Dawley rats (8–10 weeks old, 200–250 g; Animalario General University of Santiago de Compostela [USC]) and adult male null SF1-Cre AMPKα1$^{flox/flox}$ mice (mixed background; 20 weeks old for the standard diet [SD] experiments and 34 weeks old for the HFD experiments) and their littermates were used. All experiments were performed in agreement with the International Law on Animal Experimentation and were approved by the USC Ethical Committee (project ID 15010/14/006) and the University of Iowa Institutional Animal Care and Use Committee. To generate SF1 neuron-specific AMPKα1 knockout mice (SF1-Cre AMPKα1$^{flox/flox}$), SF1-Cre mice [Tg(Nr5a1-cre)Lowl/J, stock number 012462] were crossed with AMPKα1 floxed mice (AMPKα1$^{flox/flox}$ mice, Prkaa1tm1.1Sjm/J, stock number 014141; both strains from The Jackson Laboratory, Bar Harbor, ME) that possess loxP sites flanking exon 3 of the *Prkaa1* gene. Cre-negative, floxed (AMPKα1$^{flox/flox}$) littermates were used as controls (10). The animals were housed with an artificial 12-h light (0800 h to 2000 h)/12-h dark cycle, under controlled temperature and humidity conditions and allowed free access to standard laboratory chow (SAFE A04; Scientific Animal Food & Engineering, Nantes, France) or 45% HFD (D12451; Research Diets, Inc., New Brunswick, NJ) and tap water.

Generation of Lentiviral Particles

The protein-coding sequence of AMPKα1-DN was cloned from pVQAd Sf1-AMPKα1-DN (Material serial reference number [MSRN] 24603; ViraQuest Inc., North Liberty, IA) into the pSIN-Flag vector. To generate lentiviral (Lv) particles, the pSIN-Flag vector containing AMPKα1-DN was cotransfected with packaging vectors (psPAX2 and pMD2G) into HEK293T as previously described (21). pMD2G and psPAX2 were a gift from Didier Trono (12259 and 12260, respectively; Addgene Plasmids, Cambridge, MA).

Stereotaxic Microinjection of Viral Vectors

Adenoviral (GFP, AMPKα1-DN, AMPKα2-DN, and AMPKα1-CA; Viraquest) and Lv (null and AMPKα1-DN) vectors were delivered in the VMH of rats or mice as previously reported (7,10,11,13–16,22,23).

Peripheral Treatments

The adrenergic receptor β3 (β3-AR)–specific antagonist SR59230A (3 mg/kg/day; Tocris Bioscience, Bristol, U.K.) was administrated subcutaneously (SC), as previously reported (7,10,11,24).

Glucose and Insulin Tolerance Tests

Glycemia was measured with a glucometer (Accucheck; Roche, Barcelona, Spain) after insulin or glucose administration, after an intraperitoneal injection of 0.75 units/kg insulin (Actrapid; Novonordisk, Bagsvaerd, Denmark) for insulin tolerance test or 1 mg/g D-glucose (Sigma-Aldrich, St. Louis, MO) for glucose tolerance test, as previously shown (23,24). HOMA of insulin resistance (HOMA-IR) was calculated as previously reported (24).

Calorimetric System and Nuclear Magnetic Resonance

Animals were analyzed for EE, oxygen consumption (VO_2), respiratory quotient (RQ), and locomotor activity (LA) using a calorimetric system (LabMaster; TSE Systems, Bad Homburg, Germany) as previously shown (10,11,13,16).

Positron Emission Tomography–Computed Tomography

Whole-body microPET/CT (positron emission tomography–computed tomography) images were acquired with the Albira PET/CT Preclinical Imaging System (Bruker Biospin, Woodbridge, CT). Mice received an injection of 7.4 ± 1.85 MBq of 2-^{18}F-fluoro-2-deoxy-2-glucose (^{18}F-FDG) in the tail vein. The acquisition was performed 45 ± 10 min after the ^{18}F-FDG injections. Images were generated using the Bruker Albira Suite software, version 5.0. The brown fat and liver areas were delineated by using image tools implemented in the AMIDE software (http://amide.sourceforge.net/) to generate a three-dimensional spherical volume of interest with a radius of 6 mm. Thus, mean standardized uptake values were calculated (10).

BAT Temperature Measurements

Skin temperature surrounding BAT was recorded with an infrared camera (B335, Compact Infrared Thermal Imaging Camera; FLIR, West Malling, Kent, U.K.) as previously shown (10,11,13,14,16,23,24).

Sympathetic Nerve Activity Recording

Multifiber recording of sympathetic nerve activity (SNA) was obtained from the nerve subserving BAT as previously described (7,10,11,14,23).

Sample Processing

From each animal, the VMH, BAT, subcutaneous WAT (scWAT), and liver were immediately homogenized on ice to preserve phosphorylated protein levels. Samples were stored at −80°C until further processing. The specificity of the VMH dissections was confirmed by analyzing the mRNA of SF1 and proopiomelanocortin (POMC) (data not shown).

Blood Biochemistry

Levels of insulin and leptin were measured using mice ELISA kits (Merck Millipore, Billerica, MA), triglyceride

and cholesterol were measured using Spinreact kits (Spinreact S.A., San Esteve de Bas, Spain), and nonesterified fatty acids (NEFAs) were measured using the Wako kit (Wako Chemicals GmbH, Neuss, Germany) on fed animals. Plasma glucagon levels were measured using a mouse ELISA kit (Mercodia AB, Uppsala, Sweden), corticosterone (CORT) levels were analyzed using a competitive enzyme immunoassay kit (Enzo Life Sciences, Farmingdale, NY), and epinephrine levels were measured using an ELISA kit (CUSABIO, Houston, TX) in 24 h–fasted HFD mice.

Real-time Quantitative RT-PCR

Real-time PCR (TaqMan; Applied Biosystems, Foster City, CA) was performed using specific primers and probes (Supplementary Table 1) as previously described (7,10, 11,16,23).

Immunohistochemistry

Detection of uncoupling protein 1 (UCP1) in WAT was performed using anti-UCP1 (1:500, ab10983; Abcam, Cambridge, U.K.) as previously reported (24–26). Digital images for WAT were quantified with ImageJ Software (National Institutes of Health [NIH], Bethesda, MD), as previously shown (24–26). Direct detection of GFP fluorescence was performed as previously reported (10,24,26).

Double Immunohistochemistry/In Situ Hybridization

In situ hybridization analysis was performed as previously shown (27) using a specific antisense riboprobe complementary to the coding sequence of the whole exon 3 of mice *Prkaa1* mRNA (*PrKaa1*-ex3 riboprobe, 278- and 371-nt, NM_001013367.3). For the generation of the template, primer sequences were as follows: forward T3-AMPKex3-sense (5′-CAGAGATGCAATTAACCCTCACTAAAGGGAGAGTACCAGGTCATCAGTACACCATCT-3′); reverse T7-AMPKex3-as (5′-CCAAGCCTTCTAATACGACTCACTATAGGGAGACCTTCCATTTTTACAGATATAATCA-3′). After hybridization, sections were processed for immunohistochemistry of SF1 with anti-SF1 antibody (1:500; Abcam). Brain sections were incubated against a biotinylated donkey anti-rabbit secondary antibody (1:500; Jackson ImmunoResearch Laboratories, West Grove, PA), and peroxidase reaction was performed using the VECTASTAIN Elite ABC-HRP Kit (Vector Laboratories, Burlingame, CA) and 3,3′-diaminobenzidine-tetrahydrochloride (DAB). Slides were dipped in Kodak Autoradiography Emulsion type NTB (Kodak, Rochester, NY) and exposed for 3 weeks at 4°C in the dark. After this period, the sections were developed and fixed.

Western Blotting

Protein lysates from the VMH, BAT, and liver were subjected to SDS-PAGE, electrotransferred, and probed with antibodies against acetyl-CoA carboxylase α (ACCα), AMPKα2 (Merck Millipore), phosphorylated ACCα (pACCα; Ser79), phosphorylated hormone-sensitive lipase (pHSL; Ser660), tumor necrosis factor α (TNF-α), and forkhead box protein O1 (FOXO1) and its phosphorylated form (pFOXO1) (Cell Signaling, Danvers, MA), activating transcription factor 6 β (ATF6β), CHOP, nuclear factor-κB (NF-κB) p65, phosphorylated IkB kinase α/β (p-IKKα/β), phosphorylated protein kinase RNA-like endoplasmic reticulum kinase (pPERK; Thr981), glucokinase (GCK) (Santa Cruz Biotechnology, Dallas, TX), HSL, interleukin 1β (IL-1β), interleukin 6 (IL-6), phosphorylated inositol-requiring enzyme 1 (pIREα; Ser724), UCP1, glucose-6-phosphatase (G6pase), pyruvate carboxykinase (PCK1) (Abcam), α-tubulin, or β-actin (Sigma-Aldrich), as previously described (7,10,11,14,23,24). Autoradiographic films (Fujifilm, Tokyo, Japan) were scanned and the band signal was quantified by densitometry using ImageJ 1.33 software (NIH), as previously shown (7,10,11,13–16,22,23). Values were expressed in relation to β-actin (VMH) or α-tubulin (BAT). Representative images for all proteins are shown; in the case of the loading controls, a representative gel is displayed, although each protein was corrected by its own internal control (β-actin or α-tubulin). In all the figures showing images of gels, all the bands for each picture are from the same gel, although they may be spliced for clarity.

Statistical Analysis

Data are expressed as mean ± SEM; when data are relativized, they are given as percentage of the appropriate controls. Error bars represent SEM. Statistical significance was determined by Student *t* test (when two groups were compared) or ANOVA (when more than two groups were compared) followed by post hoc Bonferroni test. $P < 0.05$ was considered significant; the exact *P* values are specified in the RESULTS.

RESULTS

Inhibition of AMPKα in the VMH Reverses HFD-Induced Obesity

We stereotaxically injected into the VMH of HFD-induced obese rats a combination of adenoviruses harboring dominant-negative isoforms of the catalytic AMPKα1 and α2 (AMPKα1α2-DN) subunits. The infection efficiency was demonstrated by assaying the hypothalamic expression of GFP into the VMH (Fig. 1*A*), as previously reported (7,10,11,13,14,16,22). Treatment with an adenovirus expressing AMPKα1α2-DN induced a feeding-independent weight loss in rats fed HFD (day 1 $P = 0.004$, day 2 $P = 0.0006$, day 3 $P = 0.00007$, day 4 $P = 0.00007$, day 5 $P = 0.00001$) (Fig. 1*B* and *C*) and SD controls (day 1 $P = 0.08$, day 2 $P = 0.014$, day 3 $P = 0.001$, day 4 $P = 0.0001$, day 5 $P = 0.0002$) (Supplementary Fig. 1*A* and *B*). This effect was associated with VMH decreased levels of pACCα (HFD $P = 0.04$, SD $P = 0.005$) and/or endoplasmic reticulum (ER) stress markers (pIRE $P = 0.009$, pPERK $P = 0.04$, ATF6β $P = 0.0007$) (Fig. 1*D* and *E* and Supplementary Fig. 1*C*). AMPKα1α2-DN elicited an increase in BAT temperature ($P = 0.04$) (Fig. 1*F*) as well as in the protein ($P = 0.001$) and/or mRNA expression ($P = 0.01$) of UCP1 and peroxisome proliferator–activated receptor-γ coactivator 1α ($P = 0.01$) and 1β ($P = 0.06$) (PGC1α and PGC1β) in the BAT

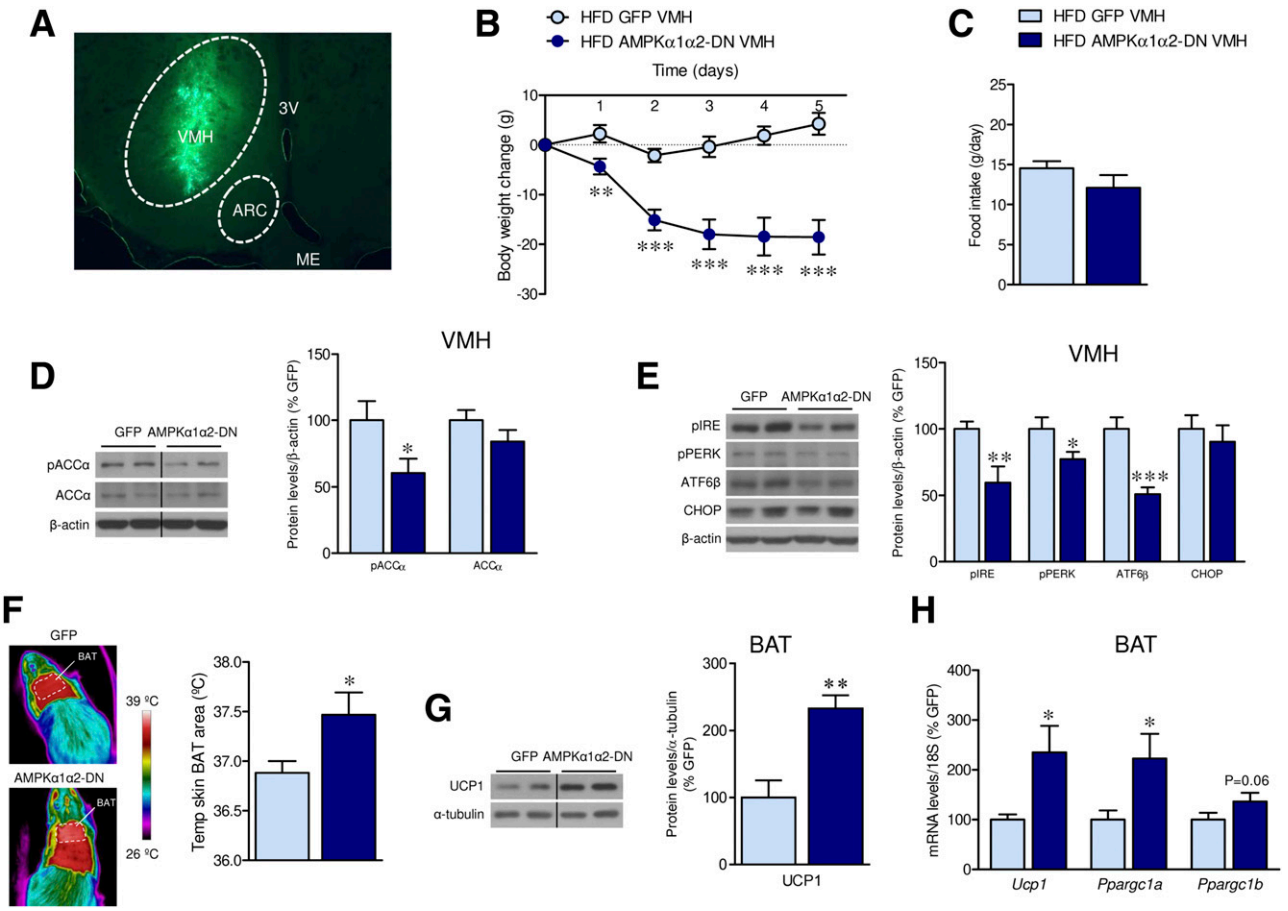

Figure 1—Effect of AMPKα1α2-DN microinjection into the VMH on energy balance in HFD-induced obese rats. *A*: Representative image of direct GFP fluorescence in the VMH after injection of adenovirus. *B*: Body weight change (n = 9 rats/group). *C*: Daily food intake (n = 9 rats/group). *D*: Protein levels of pACCα and ACCα in the VMH (n = 7 rats/group). *E*: Protein levels of the ER stress pathway in the VMH (n = 7 rats/group). *F*: BAT temperature (n = 7 rats/group). *G*: Protein levels of UCP1 in the BAT (n = 7 rats/group). *H*: mRNA levels of thermogenic markers in the BAT (n = 9 rats/group) of rats fed an HFD stereotaxically treated within the VMH with GFP or AMPKα1-DN and AMPKα2-DN adenoviruses. $^*P < 0.05$, $^{**}P < 0.01$, and $^{***}P < 0.001$ vs. HFD GFP VMH. Statistical significance was determined by Student t test. Data expressed as mean ± SEM. The bands in gels from panels *D*, *E*, and *G* have been spliced from the same original gels, as indicated by vertical black lines. ME, medial eminence.

of HFD-fed rats (Fig. 1*G* and *H*). These data indicate that inhibition of AMPKα within the VMH decreases DIO.

Specific Inhibition of AMPKα1 Isoform in the VMH Reverses HFD-Induced Obesity

Next, we treated rats stereotaxically within the VMH with adenoviruses expressing AMPKα1-DN or AMPKα2-DN. Although both isoforms induced a significant decrease in body weight (AMPKα1-DN: day 1 P = 0.01, day 2 P = 0.018, day 3 P = 0.04, day 4 P = 0.008, day 5 P = 0.005; AMPKα2-DN: day 1 P = 0.03, day 2 P = 0.07, day 3 P = 0.06, day 4 P = 0.02, day 5 P = 0.01), AMPKα1-DN, but not AMPKα2-DN, caused a feeding-independent weight loss (AMPKα2-DN P = 0.03) (Fig. 2*A*–*C*). Since BAT thermogenesis is mainly controlled by the SNS via β3-AR (28), we investigated whether BAT activity after administration of AMPKα1-DN or AMPKα2-DN adenoviral particles in the VMH was mediated by the SNS. Pharmacological inactivation of β3-AR by SC administration of SR59230A (7,10,11,24) prevented the effect on BAT (ANOVA P = 0.018, F = 4.45; GFP vs. AMPKα1-DN P = 0.007; AMPKα1-DN vs. AMPKα1-DN + SR59230A P = 0.04) (Fig. 2*D*) and body temperature (ANOVA P = 0.0084, F = 5.35; GFP vs. AMPKα1-DN P = 0.006; AMPKα1-DN vs. AMPKα1-DN + SR59230A P = 0.002) (Fig. 2*E*) associated with AMPKα1-DN injection into the VMH. Consistent with the increased thermogenesis, the treatment with SR59230A blunted the weight-reducing effect of AMPKα1-DN (GFP −9.76 ± 2.62 g, AMPKα1-DN −21.86 ± 3.71 g, $P < 0.01$ vs. GFP; AMPKα1-DN + SR59230A −12.71 ± 2.93 g, $P < 0.05$ vs. AMPKα1-DN).

Next, we evaluated the impact of AMPKα1-DN in rats fed an HFD. Administration of AMPKα1-DN adenovirus into the VMH of HFD-induced obese rats induced feeding-independent weight loss (day 1 P = 0.04, day 2 P = 0.002, day 3 P = 0.006, day 4 P = 0.006, day 5 P = 0.001) (Fig. 2*F* and *G*), associated with increased BAT temperature (P = 0.0004) (Fig. 2*H*). Since our adenoviral treatments lasted 5 days, which correspond to the maximal effect of

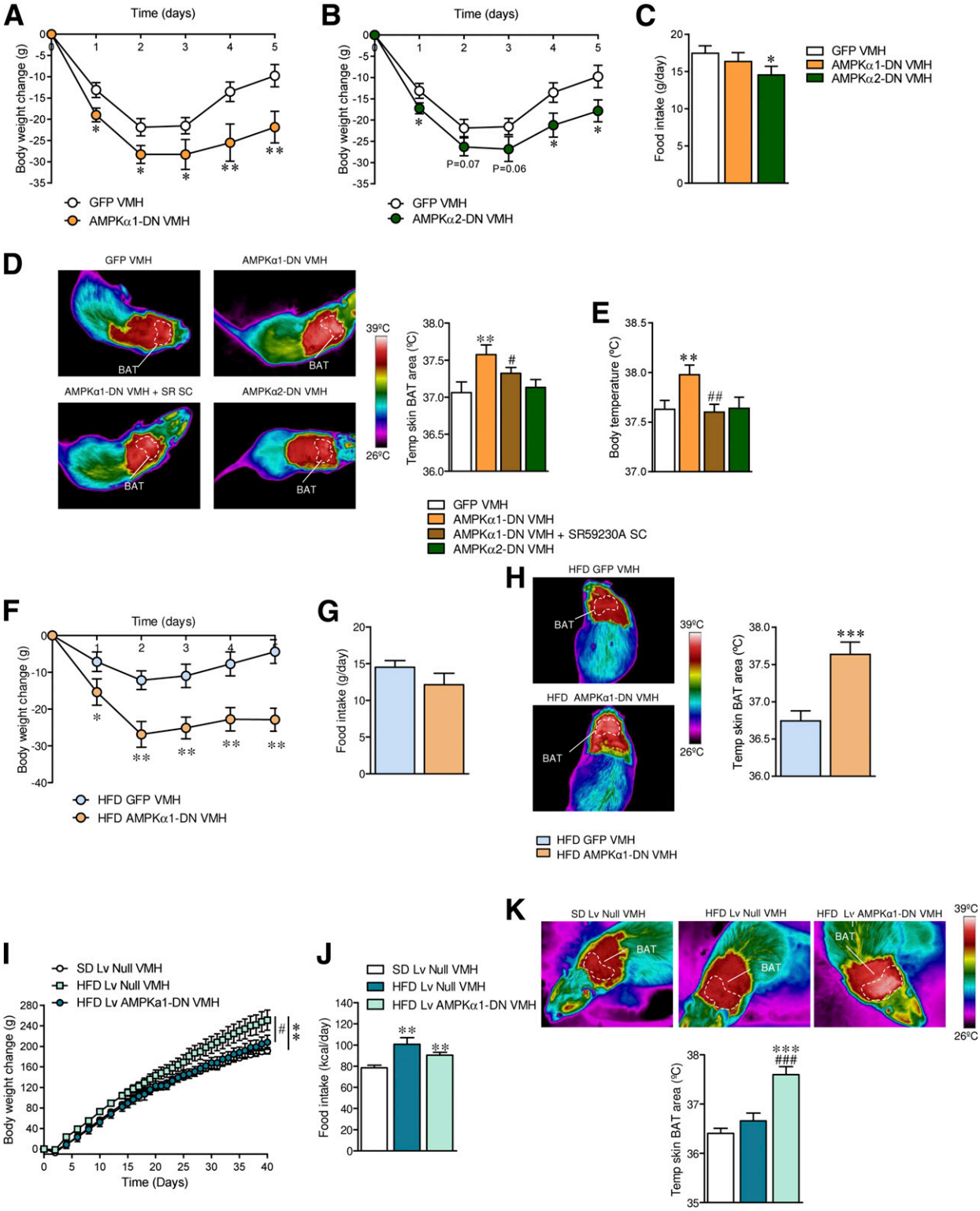

Figure 2—Effect of AMPKα1-DN or AMPKα2-DN microinjection into the VMH on energy balance in rats. *A* and *B*: Body weight change (n = 14–17 rats/group). *C*: Daily food intake (n = 14–17 rats/group). *D*: BAT temperature (n = 14–17 rats/group). *E*: Body temperature (n = 14–17 rats/group) of rats fed an SD stereotaxically treated within the VMH with GFP or AMPKα1-DN or AMPKα2-DN adenoviruses and SC with SR59230A (SR SC). *F*: Body weight change (n = 16–19 rats/group). *G*: Daily food intake (n = 16–19 rats/group). *H*: BAT temperature (n = 8 rats/group) of rats fed an HFD stereotaxically treated within the VMH with GFP or AMPKα1-DN adenoviruses. *I*: Body weight change (n = 7–8 rats/group). *J*: Food intake (n = 7–8 rats/group). *K*: BAT temperature (n = 7–8 rats/group) of rats fed an HFD stereotaxically treated within the VMH with null or AMPKα1-DN Lv. $^{*}P < 0.05$, $^{**}P < 0.01$, and $^{***}P < 0.001$ vs. GFP VMH or null VMH. $\#P < 0.05$, $\#\#P < 0.01$, and $\#\#\#P < 0.001$ vs. AMPKα1-DN VMH. Statistical significance was determined by Student t test (when two groups were compared) or ANOVA (when more than two groups were compared) followed by post hoc Bonferroni test. Data are expressed as mean ± SEM.

the viral infection (7,10,11,14–16,22–24,26,29), we investigated the effect of virogenic targeting of AMPKα1 in HFD obese rats for a longer duration. For this purpose, we used Lv harboring the AMPKα1-DN cDNA. Lv allow the prolonged expression of the transgene due to the integration in the host genome (30). Our data show that a single VMH administration with AMPKα1-DN Lv after 40 days induced a marked feeding-independent weight loss (body weight change ANOVA $P = 0.018$, $F = 4.99$; SD Lv null vs. HFD Lv null $P = 0.005$; HFD Lv null vs. HFD Lv AMPKα1-DN $P = 0.04$; food intake ANOVA $P = 0.0043$, $F = 7.24$; SD Lv null vs. HFD Lv null $P = 0.006$; SD Lv null vs. HFD Lv AMPKα1-DN $P = 0.002$; HFD Lv null vs. HFD Lv AMPKα1-DN $P = 0.2$ [nonsignificant]) (Fig. 2*I* and *J*). Importantly, this was associated with increased BAT thermogenesis in HFD animals, which lasted during the 40-day time period (ANOVA $P = 0.00002$, $F = 20.19$; HFD Lv null vs. HFD Lv AMPKα1-DN $P = 0.0007$) (Fig. 2*K*). Together, these data indicated that AMPKα1, but not AMPKα2, is the key isoform modulating BAT thermogenesis within the VMH and that its inhibition decreases HFD-induced obesity.

Ablation of AMPKα1 in SF1 Neurons of the VMH Increases BAT Thermogenesis and EE

Next, we aimed to identify the specific VMH neuronal population of neurons mediating those effects. To this end, we generated a SF1-specific AMPKα1 null mouse line (SF1-Cre AMPKα1$^{flox/flox}$) (10) by crossing floxed AMPKα1 mice (31) with SF1-Cre mice, which express Cre recombinase under the SF1 promoter (32). Allele-specific PCR demonstrated the successful ablation of AMPKα1 in the VMH, a hypothalamic area highly enriched for SF1 neurons, whereas no evidence for ablation of this allele was detected in the cerebral cortex or the cerebellum (Fig. 3*A*). In addition, AMPKα1 allele ablation was detected in peripheral tissues where SF1 is also expressed, such as the adrenal gland, the pituitary, and the testis, but not in SF1-negative tissues, such as the liver (Fig. 3*A*). To further characterize the SF1-specific deletion of AMPKα1 in the VMH, we performed a dual procedure for simultaneous detection of SF1 immunoreactivity and AMPKα1 mRNA, the latter using a probe directed against the deleted sequence of the allele (flanked by the *lox-P* sites). Unambiguous colocalization of AMPKα1 mRNA was detected in a substantial proportion of SF1 neurons in the VMH. In contrast, this proportion significantly dropped to nearly negligible levels in SF1-Cre AMPKα1$^{flox/flox}$ mice, therefore confirming the effective ablation of AMPKα1 in SF1 neurons of the VMH. This was further confirmed by quantification, showing the low degree of colocalization of AMPKα1 mRNA and SF1-positive staining in the null mice (only 11.26%) in relation to WT littermates ($P = 2.10^{-9}$) (Fig. 3*B*). Next, we investigated the effect of AMPKα1 deletion on hypothalamic AMPKα2; SF1-Cre AMPKα1$^{flox/flox}$ mice exhibited a significant upregulation of the AMPKα2 isoform within the VMH, likely to compensate for the deficiency in AMPKα function ($P = 0.02$) (Fig. 3*C*).

Interestingly, SF1-Cre AMPKα1$^{flox/flox}$ mice displayed reduced body weight (week 4 $P = 0.02$, week 8 $P = 0.001$, week 12 $P = 0.003$, week 16 $P = 0.005$, week 20 $P = 0.02$) (Fig. 3*D*) and adiposity ($P = 0.009$) (Fig. 3*E*). Body length was comparable between SF1-Cre AMPKα1$^{flox/flox}$ mice and littermate controls (Fig. 3*F*). Food intake was also not different in SF1-Cre AMPKα1$^{flox/flox}$ mice (Fig. 3*G*). SF1-Cre AMPKα1$^{flox/flox}$ mice exhibited higher EE and VO_2 ($P < 0.001$) (Fig. 3*H–I*). LA was decreased ($P = 0.007$–0.04) (Fig. 3*J*), whereas RQ remained unchanged (Fig. 3*K*). Analysis of plasma levels showed lower triglycerides ($P = 0.04$), NEFAs ($P = 0.02$), and leptin ($P = 0.005$), but unchanged cholesterol (Fig. 3*L–O*), in SF1-Cre AMPKα1$^{flox/flox}$ mice.

In keeping with the increased EE, SF1-Cre AMPKα1$^{flox/flox}$ showed BAT activation, as demonstrated by elevated SNA subserving this tissue ($P = 0.002$) (Fig. 4*A*) and the increased BAT temperature ($P = 0.008$) (Fig. 4*B*), UCP1 protein expression ($P = 0.008$) (Fig. 4*C*), and higher ^{18}F-FDG uptake in the BAT, when compared with liver ($P = 0.03$) (Fig. 4*D*), indicating higher BAT function. Of note, pharmacological inactivation of β3-AR by SC administration of SR59230A (7,10,11,24) reverted the weight loss ($P = 0.004$) in a feeding-independent manner and decreased BAT temperature ($P = 0.0009$) of SF1-Cre AMPKα1$^{flox/flox}$ mice (Supplementary Fig. 2*A–C*). Finally, SF1-Cre AMPKα1$^{flox/flox}$ mice displayed higher expression of thermogenic markers in scWAT (*Ucp1* $P = 0.007$, *Ppargc1a* $P = 0.04$, *Ppargc1b* $P = 0.01$, *Cidea* $P = 0.005$) (Supplementary Fig. 3*A*), which was indicative of browning.

SF1 is also expressed in peripheral organs. Therefore, it is possible that the phenotype of SF1-Cre AMPKα1$^{flox/flox}$ mice may be driven by the loss of AMPKα1 in those tissues. To investigate this possibility, SF1-Cre AMPKα1$^{flox/flox}$ mice were treated with an adenovirus encoding a constitutively active AMPKα1 (AMPKα1-CA) into the VMH. This gain-of-function treatment promoted feeding-independent weight gain of SF1-Cre AMPKα1$^{flox/flox}$ mice (day 1 $P = 0.09$, day 2 $P = 0.15$, day 3 $P = 0.05$, day 4 $P = 0.02$, day 5 $P = 0.002$) (Fig. 4*E* and *F*), associated with decreased BAT temperature ($P = 0.04$) (Fig. 4*G*) and UCP1 expression ($P = 0.01$) (Fig. 4*H*). Finally, SF1-Cre AMPKα1$^{flox/flox}$ mice were exposed to 4°C for 6 h. This cold challenge demonstrated that null mice defended their body temperature (2 h $P = 0.009$, 3 h $P = 0.011$, 4 h $P = 0.011$, 5 h $P = 0.02$, 6 h $P = 0.02$) (Fig. 4*I*), average body temperature ($P = 0.003$) (Fig. 4*J*), and BAT temperature (Fig. 4*K*) (0 h $P = 0.01$, 2 h $P = 0.003$, 3 h $P = 0.02$, 4 h $P = 0.01$, 5 h $P = 0.003$) (Fig. 4*K*) better than the littermate controls. Overall, this evidence demonstrated that specific ablation of AMPKα1 in SF1 neurons of the VMH promoted a negative energy balance through a process that involved activation of BAT thermogenesis and subsequent increase in EE.

SF1 AMPKα1 Null Mice Are Resistant to HFD-Induced Obesity

We evaluated whether SF1-Cre AMPKα1$^{flox/flox}$ mice were protected against obesity. Conditional null mice fed an

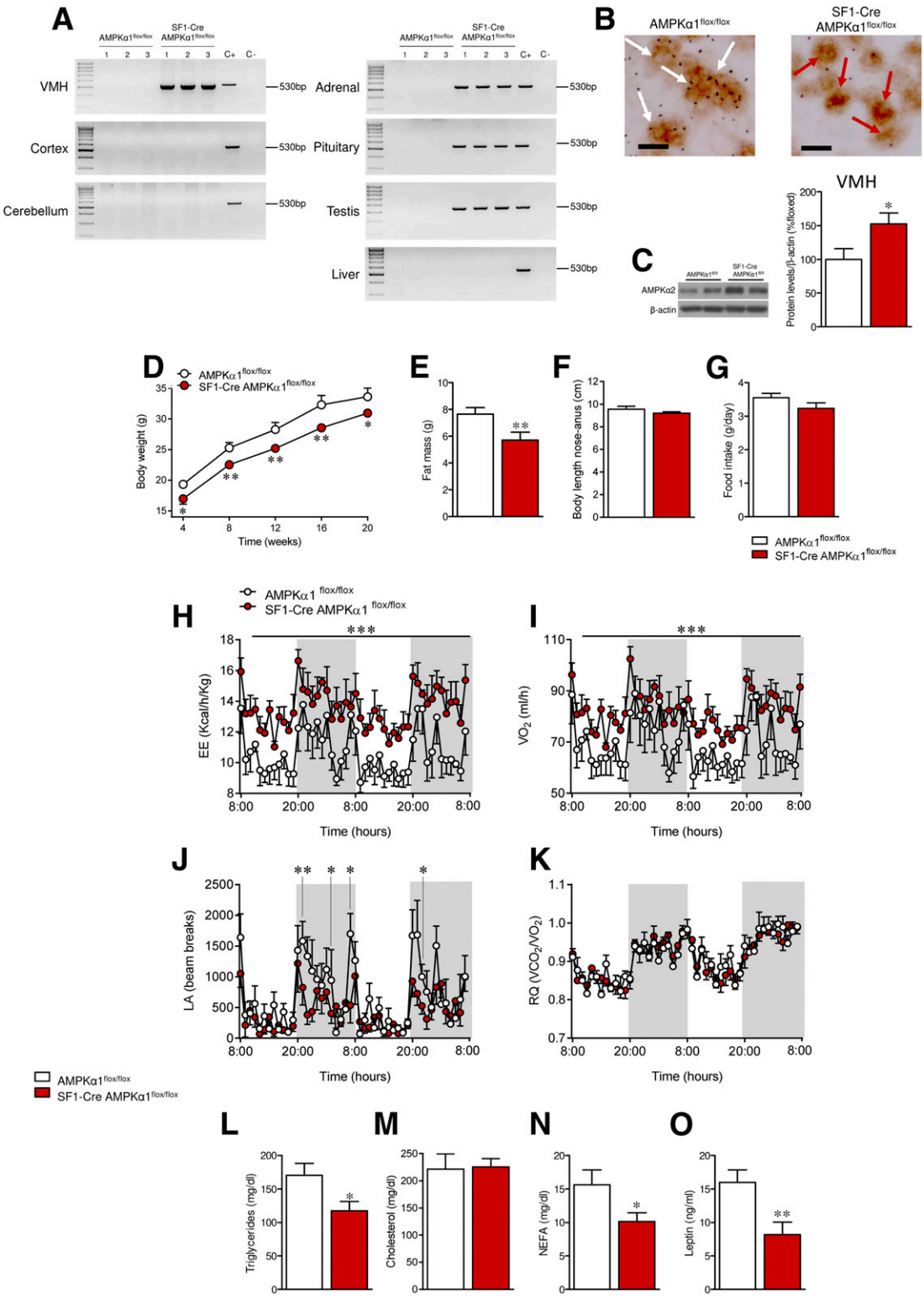

Figure 3—Effect of AMPKα1 deletion in SF1 neurons on energy balance in mice. *A*: PCR for detection of the recombined *Prkaa1* allele in the following tissues from AMPKα1$^{flox/flox}$ and SF1-Cre AMPKα1$^{flox/flox}$ mice: VMH, cortex, cerebellum, adrenal gland, pituitary, testis, and liver. *B*: Double immunohistochemistry/in situ hybridization against SF1 and AMPKα1, respectively, in the VMH of AMPKα1$^{flox/flox}$ and SF1-Cre AMPKα1$^{flox/flox}$ mice. White and red arrows indicate the presence and absence of colocalization, respectively. Scale bar: 20 μm. *C*: Protein levels of AMPKα2 in the VMH (n = 7 mice/group). *D*: Body weight (n = 12–23 mice/group). *E*: Fat pad mass (n = 12–23 mice/group). *F*: Body length (n = 7–8 mice/group). *G*: Daily food intake (n = 8 mice/group). *H*: EE (n = 5–6 mice/group). *I*: VO_2 (n = 5–6 mice/group). *J*: LA (n = 5–6 mice/group). *K*: RQ (n = 5–6 mice/group). *L–O*: Circulating levels of triglycerides, cholesterol, NEFAs, and leptin (n = 8–9 mice/group) of AMPKα1$^{flox/flox}$ and SF1-Cre AMPKα1$^{flox/flox}$ mice. *$P < 0.05$, **$P < 0.01$, and ***$P < 0.001$ vs. AMPKα1$^{flox/flox}$. Statistical significance was determined by Student t test. Data are expressed as mean ± SEM. The bands in gels from panels *C* come from the same original gels.

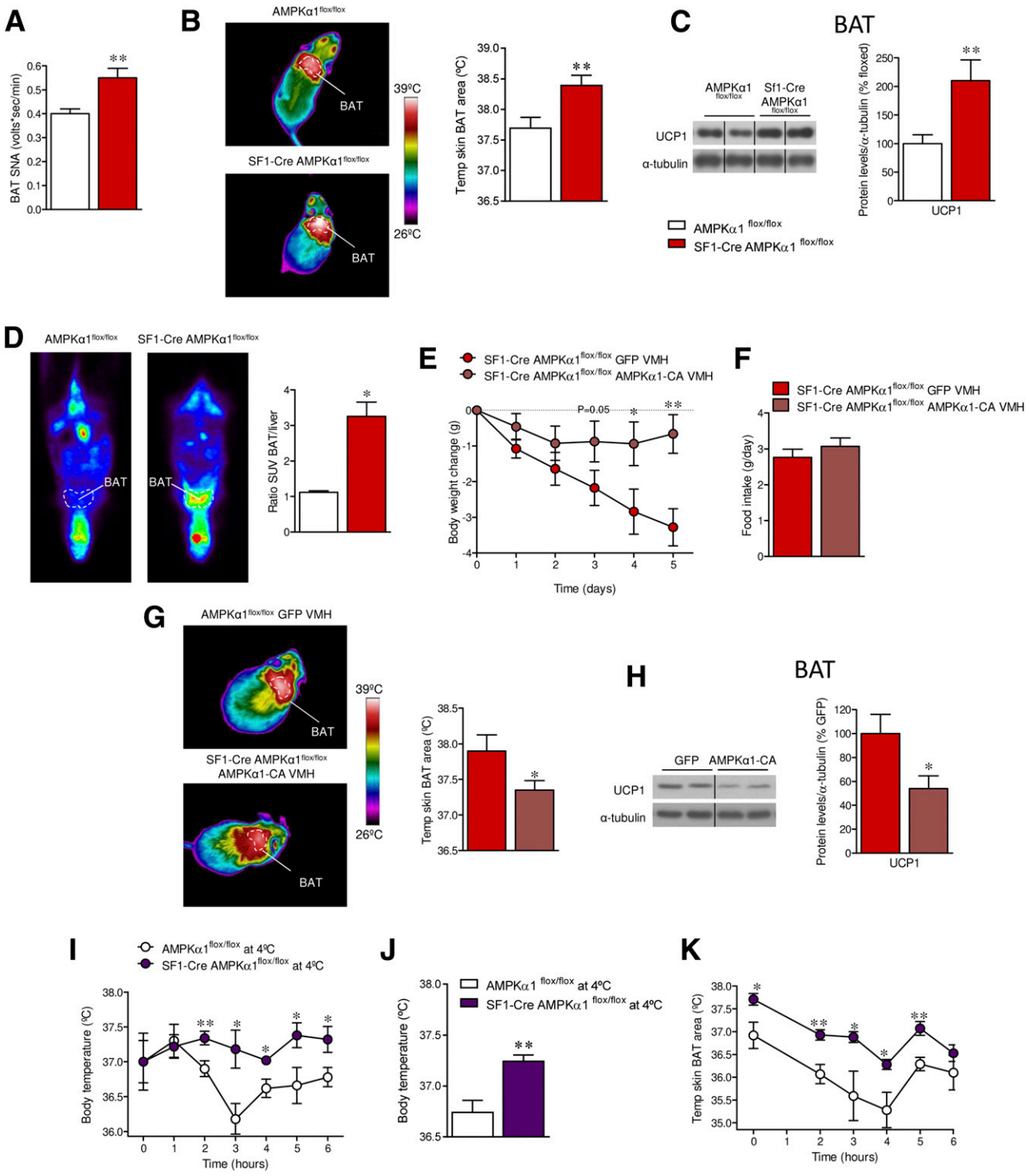

Figure 4—Effect of deleting AMPKα1 in SF1 neurons on BAT thermogenesis in mice. *A*: SNA recorded from the nerves subserving BAT (n = 8 mice/group). *B*: BAT temperature (n = 12–17 mice/group). *C*: Protein levels of UCP1 in the BAT (n = 7 mice/group). *D*: PET/CT scan (n = 6 mice/group) of AMPKα1$^{flox/flox}$ and SF1-Cre AMPKα1$^{flox/flox}$ mice. *E*: Body weight change (n = 8 mice/group). *F*: Daily food intake (n = 8 mice/group). *G*: BAT temperature (n = 8 mice/group). *H*: Protein levels of UCP1 in the BAT (n = 7 mice/group) of SF1-Cre AMPKα1$^{flox/flox}$ mice stereotaxically treated within the VMH with GFP or AMPKα1-CA adenoviruses. *I*: Body temperature (n = 5 mice/group). *J*: Average body temperature (n = 5 mice/group). *K*: BAT temperature (n = 5 mice/group) of AMPKα1$^{flox/flox}$ and SF1-Cre AMPKα1$^{flox/flox}$ mice cold challenged at 4°C for 6 h. *$P < 0.05$ and **$P < 0.01$ vs. AMPKα1$^{flox/flox}$, SF1-Cre AMPKα1$^{flox/flox}$ GFP VMH, or AMPKα1$^{flox/flox}$ at 4°C. Statistical significance was determined by Student t test. Data are expressed as mean ± SEM. The bands in gels from panels *C* and *H* have been spliced from the same original gels, as indicated by vertical black lines. SUV, standardized uptake value.

HFD showed a feeding-independent decrease in body weight (P = 0.006) and adiposity (scWAT, P = 0.02) (Fig. 5*A–D*), associated with increased EE ($P < 0.05$–0.001) and VO_2 ($P < 0.05$–0.01) (Fig. 5*E* and *F*), a slight tendency of elevated LA (Fig. 5*G*), and no change in RQ (Fig. 5*H*). Plasmatic levels of NEFAs (P = 0.005) and leptin (P = 0.03), but neither triglycerides nor cholesterol, were decreased in SF1-Cre AMPKα1$^{flox/flox}$ fed an HFD (Fig. 5*I–L*).

Analysis of the hypothalami of SF1-Cre AMPKα1$^{flox/flox}$ mice fed an HFD demonstrated decreased pACCα levels in the VMH (P = 0.04) (Fig. 6*A*). Recent evidence demonstrated that hypothalamic inflammation and ER stress induce obesity and inhibit BAT thermogenesis and browning of WAT (23,24,26,33–35). Our result showed reduced ER stress (pIRE P = 0.02, pPERK $P = 1 \times 10^{-5}$, ATF6β P = 0.01, CHOP P = 0.03) (Fig. 6*B*) and inflammatory markers (IL-1β P = 0.02, pIKKαβ P = 0.001, NF-κB P = 0.04) (Fig. 6*C*) in the VMH of HFD-fed SF1-Cre AMPKα1$^{flox/flox}$ mice. Notably, this effect was associated with higher BAT temperature ($P = 1 \times 10^{-6}$) (Fig. 6*D*) and elevated mRNA or protein expression of thermogenic markers, such as UCP1, PGC1β (*Ucp1* P = 0.0015, *Ucp3* P = 0.06, *Ppargc1b* P = 0.015, UCP1 protein P = 0.005), and pHSL (P = 0.0005, pHSL/HSL

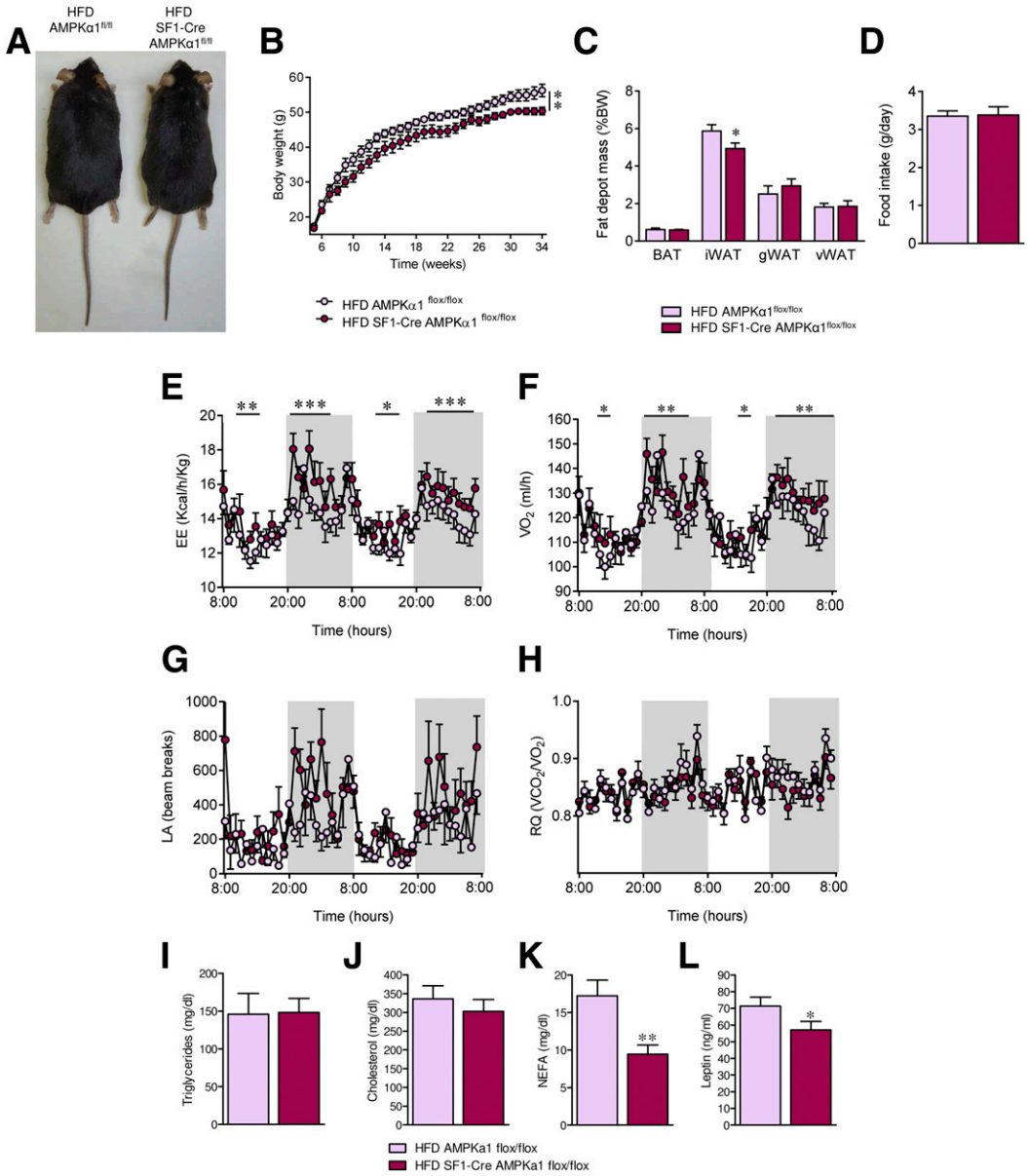

Figure 5—Effect of AMPKα1 deletion in SF1 neurons on HFD-induced obesity in mice. *A*: Representative pictures of mice. *B*: Body weight (n = 10–11 mice/group). *C*: Fat pad mass (n = 10–11 mice/group). *D*: Daily food intake (n = 10–11 mice/group). *E*: EE (n = 5–8 mice/group). *F*: VO_2 (n = 5–8 mice/group). *G*: LA (n = 5–8 mice/group). *H*: RQ (n = 5–8 mice/group). *I–L*: Circulating levels of triglycerides, cholesterol, NEFAs, and leptin (n = 8–9 mice/group) of AMPKα1$^{flox/flox}$ and SF1-Cre AMPKα1$^{flox/flox}$ mice fed an HFD. *$P < 0.05$, **$P < 0.01$, and ***$P < 0.001$ vs. HFD AMPKα1$^{flox/flox}$. Statistical significance was determined by Student t test. Data are expressed as mean ± SEM. gWAT, gonadal WAT; iWAT, inguinal WAT; vWAT, visceral WAT.

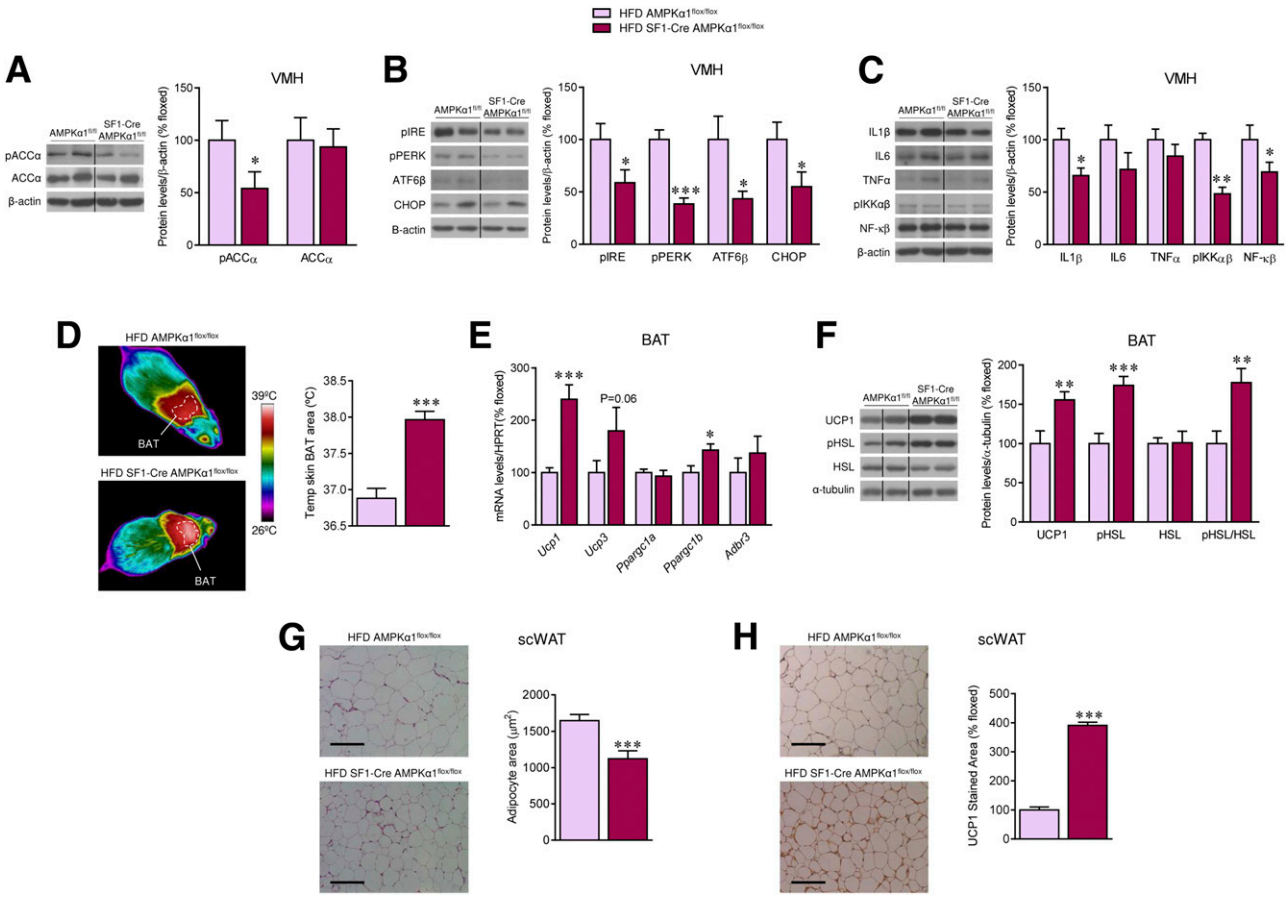

Figure 6—Effect of deleting AMPKα1 in SF1 neurons on the hypothalamus and BAT of HFD-induced obese mice. *A*: Protein levels of pACCα and ACCα in the VMH (n = 7 mice/group). *B*: Protein levels of ER stress pathway in the VMH (n = 7 mice/group). *C*: Protein levels of inflammatory markers in the VMH (n = 7 mice/group). *D*: BAT temperature (n = 10 mice/group). *E*: mRNA levels of thermogenic markers in the BAT (n = 9 rats/group). *F*: Protein levels of thermogenic markers in the BAT (n = 7 mice/group). *G*: Hematoxylin-eosin staining (left panels, scale bar: 100 μm) and adipocyte area (right panels) in scWAT (n = 11–15 mice/group). *H*: UCP1 staining (left panels, scale bar: 100 μm) and UCP1 stained area (right panels) in scWAT (n = 8–11 mice/group) of AMPKα1$^{flox/flox}$ and SF1-Cre AMPKα1$^{flox/flox}$ mice fed an HFD. *$P < 0.05$, **$P < 0.01$, and ***$P < 0.001$ vs. HFD AMPKα1$^{flox/flox}$. Statistical significance was determined by Student t test. Data are expressed as mean ± SEM. The bands in gels from panels *A–C* and *F* have been spliced from the same original gels, as indicated by vertical black lines. Original magnification ×20. HPRT, hypoxanthine-guanine phosphoribosyltransferase 1.

P = 0.003) (Fig. 6*E* and *F*) in BAT, as well as browning of scWAT, as indicated by decreased adipocyte area (P = 0.0007) (Fig. 6*G*) and increased UCP1 staining ($P = 1 \times 10^{-12}$) (Fig. 6*H*).

SF1 AMPKα1 Null Mice Show Improved Glucose Homeostasis

Finally, we evaluated the impact of AMPKα1 ablation in SF1 neurons on peripheral glucose homeostasis in the context of obesity. HFD SF1-Cre AMPKα1$^{flox/flox}$ mice showed decreased glucose levels in the fast and fed states (fast P = 0.001, fed P = 0.004) (Fig. 7*A*), improved glucose tolerance (0 min P = 0.009, 15 min P = 0.05, 30 min P = 0.07, 60 min P = 0.004, 90 min P = 0.006, 120 min P = 0.003, area under the curve [AUC] P = 0.004) (Fig. 7*B* and *C*), and unchanged insulin sensitivity and insulin levels (Fig. 7*D–F*). HOMA-IR confirmed that HFD-induced insulin resistance was ameliorated in SF1-Cre AMPKα1$^{flox/flox}$ (P = 0.06) (Fig. 7*G*).

In this context, the lack of effect in insulin sensitivity was intriguing. It has been reported that AMPK in the VMH plays a major role in counterregulatory responses to hypoglycemia by modulating the release of glucagon, CORT, and epinephrine (5,36). Our results showed that when fasted, HFD AMPKα1 null animals displayed lower levels of glucagon (nonsignificant trend, P = 0.06), decreased CORT (P = 0.008), and no changes in epinephrine (Fig. 7*H–J*), suggesting an altered counterregulatory response and that hepatic release of glucose is likely also diminished. Finally, we examined the levels of key enzymes involved in hepatic glucose metabolism. Our data showed that the protein levels of pFOXO1 were increased, whereas the protein levels of PCK1 and G6Pase were decreased (Supplementary Fig. 4*A*), which was consistent with decreased hepatic gluconeogenesis in SF1-Cre AMPKα1$^{flox/flox}$ mice. On the other hand, the liver protein expression of GCK was increased, consistent with increased glycolysis in the liver of SF1-Cre AMPKα1$^{flox/flox}$ (Supplementary

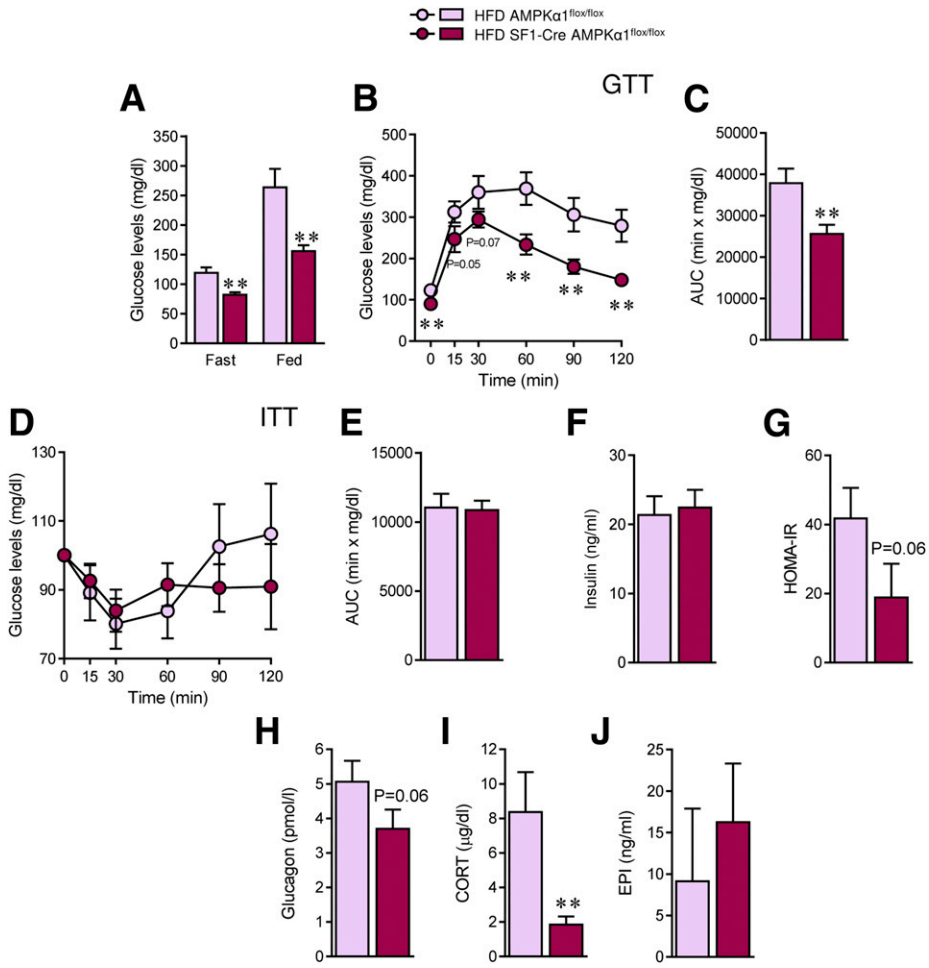

Figure 7— Effect of deleting AMPKα1 in SF1 neurons on glucose homeostasis in HFD-induced obese mice. *A*: Fast and fed plasma glucose levels (n = 9–11 mice/group). *B* and *C*: Glucose tolerance test and AUC (n = 10–11mice/group). *D* and *E*: Insulin tolerance test and AUC (n = 10–11 mice/group). *F*: Plasma insulin levels (n = 9 mice/group). *G*: HOMA-IR index (n = 5 mice/group). *H*: Glucagon fasting levels (n = 5 mice/group). *I*: CORT fasting levels (n = 5 mice/group). *J*: Epinephrine fasting levels (n = 5–6 mice/group). $^{**}P < 0.01$ vs. HFD AMPKα1$^{flox/flox}$. Statistical significance was determined by Student t test. Data are expressed as mean ± SEM. EPI, epinephrine.

Fig. 4*A*). Overall, these findings indicate that targeting of AMPKα1 in SF1 neurons not only ameliorated obesity but also reversed associated impaired glucose metabolism.

DISCUSSION

Hypothalamic AMPK has been implicated in the regulation of feeding, BAT thermogenesis, browning of WAT, muscle metabolism, hepatic function, and glucose homeostasis (8–10,19,25,26), as well as being involved in diet-induced leptin resistance (17,18). From a therapeutic perspective, this evidence is relevant since several agents with potential antiobesity and/or antidiabetic effects, such as nicotine (13,37), metformin (38), and liraglutide (15), some of which are even in clinical use, act through AMPK, either peripherally or centrally. Furthermore, the orexigenic and weight-gaining effects of antipsychotic drugs, such as olanzapine, are also mediated by hypothalamic AMPK (39). Therefore, hypothalamic AMPK might theoretically be considered an interesting target for drug development due to its potential to modulate both sides of the energy balance equation, namely food intake and EE (19,20). However, it is unclear *1*) whether specific inhibition of hypothalamic AMPK could ameliorate obesity, *2*) which AMPK isoform would be the best to target, and *3*) which neuronal AMPK-expressing population should be targeted.

Global inhibition of AMPKα1 and AMPKα2 in the VMH ameliorated ovariectomy-induced obesity in female rats (11). Moreover, it has been reported that specific ablation of AMPKα2 in POMC or agouti-related peptide (AgRP) neurons of the ARC produce opposite phenotypes. Indeed, whereas POMC AMPKα2 null mice display hyperphagia and obesity, AgRP AMPKα2 null mice were hypophagic and lean (6). Our data show that global inhibition of AMPKα1 and AMPKα2 within the VMH markedly decreased HFD-induced obesity in a feeding-independent manner involving increased BAT thermogenesis and EE. These latter effects occurred also when AMPKα1 was inhibited in the VMH of DIO rats but were not mimicked by targeting of AMPKα2. Notably, the effect

of global inhibition of both isoforms is recapitulated by selective ablation of AMPKα1 in SF1 neurons of the VMH, which play a major role in the sympathetic traffic to the BAT (10,40,41). The relevance of these data is reinforced by findings in our animal model, namely the SF1-Cre AMPKα1$^{flox/flox}$ mouse, which support our evidence demonstrating that AMPK signaling in the VMH, and specifically in SF1 neurons, is a canonical mechanism modulating energy balance (7,9–11,15,16,26,42). Importantly, our results also point to AMPKα1, but not AMPKα2, as the main catalytic AMPKα subunit in the VMH that mediates thermogenic control. This is supported by several findings. First, both thyroid hormones and estradiol decrease the expression and/or activity of AMPKα1 but not AMPKα2 (7,11,42). Second, the catabolic effects of those hormones, bone morphogenetic protein 8B (BMP8B), nicotine, and liraglutide are reversed by specific activation of AMPKα1 in the VMH (7,9–11,15,16,26,42). Third, the hypothalamic effects of the α2 subunits are frequently linked to regulation of food intake (4,6,22,43,44) and not thermogenesis, as confirmed in our current experiments involving VMH administration of AMPKα2-DN isoforms. Finally, SF1-Cre AMPKα1$^{flox/flox}$ mice exhibited a significant compensatory upregulation of the AMPKα2 isoform within the VMH; however, null mice still displayed a markedly thermogenic phenotype, indicating that the increase in AMPKα2 was unable to counteract the effect of AMPKα1 deficiency on BAT and WAT function. Overall, this evidence reinforces the idea that both AMPKα isoforms are playing different roles in the hypothalamus and that whereas AMPKα1 modulates thermogenesis, AMPKα2 does not. Further work involving the specific knockdown of α1 or α2 isoforms in other specific hypothalamic populations is warranted to better understand this pathway.

Activation of BAT and browning of WAT may represent a therapeutic strategy to combat obesity (45–47); however, the specific control of this process by a central mechanism is still unclear. Therefore, our findings showing that specific targeting of the discrete neuronal population of SF1 neurons in VMH impacts obesity by modulating thermogenesis in a feeding-independent manner is of translational relevance. Notably, that action also occurs in the absence of appetite-compensatory changes in the SF1-Cre AMPKα1$^{flox/flox}$ mice, which excludes undesired rebound effects. Regarding this, HFD SF1-Cre AMPKα1$^{flox/flox}$ mice also exhibit a clear amelioration of the diet-induced metabolic disorders, as demonstrated by improved glucose homeostasis. Although this may be related to the weight-reducing effects of AMPKα1 deletion in SF1 neurons, direct effects cannot be ruled out. The fact that these mice showed higher ^{18}F-FDG uptake analyzed by PET-CT was indicative of a primary mechanism for increased glucose clearance, likely independent of the weight-reducing factor. In keeping with this, our results showed that when fasted, SF1-Cre AMPKα1$^{flox/flox}$ animals displayed lower levels of glucagon and CORT, indicating an abnormal counterregulatory response to hypoglycemia. Moreover, biochemical data were consistent with decreased gluconeogenesis and increased glycolysis, and therefore lower hepatic glucose production in the liver of null mice.

Current evidence points to using multifactorial strategies for the treatment of obesity. The unimolecular combination of different compounds, such as peptide conjugates (with other peptides or steroid/thyroid hormones), has yielded very successful and promising preclinical and clinical (phases 1–2) results (48–50). These strategies target different molecules/receptors to broadly and simultaneously affect several aspects of energy homeostasis, such as feeding, EE, and glucose metabolism (48–50). The fact that hypothalamic AMPK controls all those aspects makes it an interesting and unique candidate for obesity treatment (19,20). In this sense, it has been demonstrated that AgRP AMPKα2 null mice tend to have lower body weight when exposed to an HFD (6). This suggests that the concomitant targeting of AMPKα in SF1 neurons of the VMH and AgRP neurons in the ARC may allow to control both feeding and EE by inhibiting a single molecule, namely AMPK. However, this is challenging for several reasons. First, the strategy must ensure the specific inhibition of hypothalamic AMPK given the differential regulation of this enzyme between the hypothalamus and the peripheral tissues (4,8,9,51), where it would have deleterious consequences (for example, worsening insulin resistance and diabetes). Second, the possible choices to specifically target hypothalamic AMPK seem limited. Optogenetic modulation of central AMPK has been successfully achieved in rodents (52); however, at the current stage, its implementation in clinics appears distant. The utilization of nanoparticles (53) might be an interesting option. Finally, chimeras combining glucagon-like peptide-1 (GLP-1) with estradiol (54) or glucagon with T3 (55), all of which inhibit hypothalamic AMPK (7,11,12,15), would allow targeting of hypothalamic AMPK. Further work is warranted to answer these questions.

In conclusion, our data identify the AMPKα1 isoform in SF1 neurons of the VMH as the energy sensor regulating energy balance, its inhibition being sufficient to ameliorate obesity in a feeding-independent, but thermogenic-dependent, manner. This finding also opens the need for further functional assessment of the two AMPKα isoforms in the different homeostatic processes controlled by the hypothalamus. Finally, these results suggest that targeting this energy sensor in specific sets of neurons may be a suitable strategy to combat obesity and related metabolic complications.

Acknowledgments. The PET/CT analysis was performed in the Molecular Imaging Unit of the Department of Nuclear Medicine of the USC.

Funding. The research leading to these results received funding from the Consellería de Cultura, Educación e Ordenación Universitaria, Xunta de Galicia (ED431F 2016/016 [M.F.], 2015-CP080 and 2016-PG057 [R.N.], and 2015-CP079

and 2016-PG068 [M.L.]), the Ministerio de Economía y Competitividad (MINECO) cofunded by the FEDER Program of the E.U. (BFU2016-80899-P [M.F.], BFU2014-55871-P [C.D.], BFU2015-70664R [R.N.], BFU2014-57581-P [M.T.-S.], SAF2015-71026-R [M.L.], and BFU2015-70454-REDT/Adipoplast), the NIH Clinical Center (HL084207 [K.R.]), the University of Iowa Fraternal Order of Eagles Diabetes Research Center (K.R.), the American Heart Association (EIA no. 14EIA18860041 [K.R.]), Junta de Andalucía (P12-FQM-01943 [M.T.-S.]), and the European Community's Seventh Framework Programme (FP7 Ideas: European Research Council, FP7/2007-2013) under grant agreement 281854 (the ObERStress project [M.L.]). E.R.-P. received a fellowship from MINECO (BES-2015-072743). L.L.-P. received a fellowship from Xunta de Galicia (ED481A-2016/094). M.F. received a Ramón y Cajal contract from MINECO (RYC-2014-16779). The CiMUS is supported by Xunta de Galicia (2016-2019, ED431G/05). CIBER Fisiopatología de la Obesidad y Nutrición is an initiative of ISCIII.

The funders had no role in study design, data collection and analysis, decision to publish, or preparation of the manuscript.

Duality of Interest. M.L. received funding from the Atresmedia Corporación. No other potential conflicts of interest relevant to this article were reported.

Author Contributions. P.S.-C. performed the in vivo experiments and analytical methods (nuclear magnetic resonance, blood biochemistry, RT-PCR, and Western blotting); collected, analyzed, interpreted, and discussed the data; generated and phenotyped the SF1-Cre AMPK$\alpha1^{flox/flox}$ mouse model; reviewed and edited the manuscript; made the figures; and conceived and designed the experiments. J.R. conducted part of the genotyping and characterization of the SF1-Cre AMPK$\alpha1^{flox/flox}$ mouse model; analyzed, interpreted, and discussed the data; and reviewed and edited the manuscript. E.R.-P., L.L.-P., T.L.-G., and N.M.-S. performed the in vivo experiments and analytical methods (nuclear magnetic resonance, blood biochemistry, RT-PCR, and Western blotting), collected and analyzed the data, and reviewed and edited the manuscript. D.B. and C.C. reviewed and edited the manuscript. F.R.-P. and M.J.S.-T. conducted part of the genotyping and characterization of the SF1-Cre AMPK$\alpha1^{flox/flox}$ mouse model and reviewed and edited the manuscript. D.A.M. performed and analyzed the SNA studies and reviewed and edited the manuscript. J.Á.P. and M.F. developed the Lv encoding AMPKα1-DN isoforms and reviewed and edited the manuscript. C.D., R.C., R.N., and M.T.-S. analyzed, interpreted, and discussed the data and reviewed and edited the manuscript. K.R. performed and analyzed the SNA studies; analyzed, interpreted, and discussed the data; and reviewed and edited the manuscript. M.L. analyzed, interpreted, and discussed the data; reviewed and edited the manuscript; made the figures; conceived and designed the experiments; developed the hypothesis; secured funding; coordinated and led the project; and wrote the manuscript. M.L. is the guarantor of this work and, as such, had full access to all the data in the study and takes responsibility for the integrity of the data and the accuracy of the data analysis.

References

1. Kahn BB, Alquier T, Carling D, Hardie DG. AMP-activated protein kinase: ancient energy gauge provides clues to modern understanding of metabolism. Cell Metab 2005;1:15–25

2. Carling D, Mayer FV, Sanders MJ, Gamblin SJ. AMP-activated protein kinase: nature's energy sensor. Nat Chem Biol 2011;7:512–518

3. Hardie DG. AMP-activated protein kinase: maintaining energy homeostasis at the cellular and whole-body levels. Annu Rev Nutr 2014;34:31–55

4. Minokoshi Y, Alquier T, Furukawa N, et al. AMP-kinase regulates food intake by responding to hormonal and nutrient signals in the hypothalamus. Nature 2004; 428:569–574

5. McCrimmon RJ, Fan X, Cheng H, et al. Activation of AMP-activated protein kinase within the ventromedial hypothalamus amplifies counterregulatory hormone responses in rats with defective counterregulation. Diabetes 2006;55:1755–1760

6. Claret M, Smith MA, Batterham RL, et al. AMPK is essential for energy homeostasis regulation and glucose sensing by POMC and AgRP neurons. J Clin Invest 2007;117:2325–2336

7. López M, Varela L, Vázquez MJ, et al. Hypothalamic AMPK and fatty acid metabolism mediate thyroid regulation of energy balance. Nat Med 2010;16: 1001–1008

8. Schneeberger M, Claret M. Recent insights into the role of hypothalamic AMPK signaling cascade upon metabolic control. Front Neurosci 2012; 6:185

9. López M, Nogueiras R, Tena-Sempere M, Diéguez C. Hypothalamic AMPK: a canonical regulator of whole-body energy balance. Nat Rev Endocrinol 2016; 12:421–432

10. Martínez-Sánchez N, Seoane-Collazo P, Contreras C, et al. Hypothalamic AMPK-ER stress-JNK1 axis mediates the central actions of thyroid hormones on energy balance. Cell Metab 2017;26:212–229.e12

11. Martínez de Morentin PB, González-García I, Martins L, et al. Estradiol regulates brown adipose tissue thermogenesis via hypothalamic AMPK. Cell Metab 2014;20:41–53

12. Quiñones M, Al-Massadi O, Gallego R, et al. Hypothalamic CaMKKβ mediates glucagon anorectic effect and its diet-induced resistance. Mol Metab 2015;4:961–970

13. Martínez de Morentin PB, Whittle AJ, Fernø J, et al. Nicotine induces negative energy balance through hypothalamic AMP-activated protein kinase. Diabetes 2012;61:807–817

14. Whittle AJ, Carobbio S, Martins L, et al. BMP8B increases brown adipose tissue thermogenesis through both central and peripheral actions. Cell 2012;149: 871–885

15. Beiroa D, Imbernon M, Gallego R, et al. GLP-1 agonism stimulates brown adipose tissue thermogenesis and browning through hypothalamic AMPK. Diabetes 2014;63:3346–3358

16. Martins L, Seoane-Collazo P, Contreras C, et al. A functional link between AMPK and orexin mediates the effect of BMP8B on energy balance. Cell Rep 2016; 16:2231–2242

17. Martin TL, Alquier T, Asakura K, Furukawa N, Preitner F, Kahn BB. Diet-induced obesity alters AMP kinase activity in hypothalamus and skeletal muscle. J Biol Chem 2006;281:18933–18941

18. Dagon Y, Hur E, Zheng B, Wellenstein K, Cantley LC, Kahn BB. p70S6 kinase phosphorylates AMPK on serine 491 to mediate leptin's effect on food intake. Cell Metab 2012;16:104–112

19. López M. EJE PRIZE 2017: hypothalamic AMPK: a golden target against obesity? Eur J Endocrinol 2017;176:R235–R246

20. López M, Tena-Sempere M. Estradiol effects on hypothalamic AMPK and BAT thermogenesis: a gateway for obesity treatment? Pharmacol Ther 2017;178: 109–122

21. Aguilo F, Zhang F, Sancho A, et al. Coordination of m(6)A mRNA methylation and gene transcription by ZFP217 regulates pluripotency and reprogramming. Cell Stem Cell 2015;17:689–704

22. López M, Lage R, Saha AK, et al. Hypothalamic fatty acid metabolism mediates the orexigenic action of ghrelin. Cell Metab 2008;7:389–399

23. Contreras C, González-García I, Martínez-Sánchez N, et al. Central ceramide-induced hypothalamic lipotoxicity and ER stress regulate energy balance. Cell Rep 2014;9:366–377

24. Contreras C, González-García I, Seoane-Collazo P, et al. Reduction of hypothalamic endoplasmic reticulum stress activates browning of white fat and ameliorates obesity. Diabetes 2017;66:87–99

25. Alvarez-Crespo M, Csikasz RI, Martínez-Sánchez N, et al. Essential role of UCP1 modulating the central effects of thyroid hormones on energy balance. Mol Metab 2016;5:271–282

26. Martínez-Sánchez N, Moreno-Navarrete JM, Contreras C, et al. Thyroid hormones induce browning of white fat. J Endocrinol 2017;232:351–362

27. Manfredi-Lozano M, Roa J, Ruiz-Pino F, et al. Defining a novel leptin-melanocortin-kisspeptin pathway involved in the metabolic control of puberty. Mol Metab 2016;5:844–857

28. Cannon B, Nedergaard J. Brown adipose tissue: function and physiological significance. Physiol Rev 2004;84:277–359

29. Varela L, Martínez-Sánchez N, Gallego R, et al. Hypothalamic mTOR pathway mediates thyroid hormone-induced hyperphagia in hyperthyroidism. J Pathol 2012;227:209–222
30. Mancini G, Horvath TL. Viral vectors for studying brain mechanisms that control energy homeostasis. Cell Metab 2018;27:1168–1175
31. Nakada D, Saunders TL, Morrison SJ. Lkb1 regulates cell cycle and energy metabolism in haematopoietic stem cells. Nature 2010;468:653–658
32. Dhillon H, Zigman JM, Ye C, et al. Leptin directly activates SF1 neurons in the VMH, and this action by leptin is required for normal body-weight homeostasis. Neuron 2006;49:191–203
33. Zhang X, Zhang G, Zhang H, Karin M, Bai H, Cai D. Hypothalamic IKKbeta/NF-kappaB and ER stress link overnutrition to energy imbalance and obesity. Cell 2008;135:61–73
34. Ozcan L, Ergin AS, Lu A, et al. Endoplasmic reticulum stress plays a central role in development of leptin resistance. Cell Metab 2009;9:35–51
35. Schneeberger M, Dietrich MO, Sebastián D, et al. Mitofusin 2 in POMC neurons connects ER stress with leptin resistance and energy imbalance. Cell 2013;155:172–187
36. McCrimmon RJ, Shaw M, Fan X, et al. Key role for AMP-activated protein kinase in the ventromedial hypothalamus in regulating counterregulatory hormone responses to acute hypoglycemia. Diabetes 2008;57:444–450
37. Seoane-Collazo P, Martínez de Morentin PB, Fernø J, Diéguez C, Nogueiras R, López M. Nicotine improves obesity and hepatic steatosis and ER stress in diet-induced obese male rats. Endocrinology 2014;155:1679–1689
38. Foretz M, Guigas B, Bertrand L, Pollak M, Viollet B. Metformin: from mechanisms of action to therapies. Cell Metab 2014;20:953–966
39. Skrede S, Martins L, Berge RK, Steen VM, López M, Fernø J. Olanzapine depot formulation in rat: a step forward in modelling antipsychotic-induced metabolic adverse effects. Int J Neuropsychopharmacol 2014;17:91–104
40. Lindberg D, Chen P, Li C. Conditional viral tracing reveals that steroidogenic factor 1-positive neurons of the dorsomedial subdivision of the ventromedial hypothalamus project to autonomic centers of the hypothalamus and hindbrain. J Comp Neurol 2013;521:3167–3190
41. Xu Y, Nedungadi TP, Zhu L, et al. Distinct hypothalamic neurons mediate estrogenic effects on energy homeostasis and reproduction. Cell Metab 2011;14:453–465
42. Martínez de Morentin PB, Lage R, González-García I, et al. Pregnancy induces resistance to the anorectic effect of hypothalamic malonyl-CoA and the thermogenic effect of hypothalamic AMPK inhibition in female rats. Endocrinology 2015;156:947–960
43. López M. AMPK wars: the VMH strikes back, return of the PVH. Trends Endocrinol Metab 2018;29:135–137
44. Okamoto S, Sato T, Tateyama M, et al. Activation of AMPK-regulated CRH neurons in the PVH is sufficient and necessary to induce dietary preference for carbohydrate over fat. Cell Rep 2018;22:706–721
45. Nedergaard J, Cannon B. The browning of white adipose tissue: some burning issues. Cell Metab 2014;20:396–407
46. Broeders EP, Nascimento EB, Havekes B, et al. The bile acid chenodeoxycholic acid increases human brown adipose tissue activity. Cell Metab 2015;22:418–426
47. Shan T, Xiong Y, Zhang P, et al. Lkb1 controls brown adipose tissue growth and thermogenesis by regulating the intracellular localization of CRTC3. Nat Commun 2016;7:12205
48. Finan B, Müller TD, Clemmensen C, Perez-Tilve D, DiMarchi RD, Tschöp MH. Reappraisal of GIP pharmacology for metabolic diseases. Trends Mol Med 2016;22:359–376
49. Tschöp MH, Finan B, Clemmensen C, et al. Unimolecular polypharmacy for treatment of diabetes and obesity. Cell Metab 2016;24:51–62
50. Müller TD, Finan B, Clemmensen C, DiMarchi RD, Tschöp MH. The New biology and pharmacology of glucagon. Physiol Rev 2017;97:721–766
51. Minokoshi Y, Kim YB, Peroni OD, et al. Leptin stimulates fatty-acid oxidation by activating AMP-activated protein kinase. Nature 2002;415:339–343
52. Yang Y, Atasoy D, Su HH, Sternson SM. Hunger states switch a flip-flop memory circuit via a synaptic AMPK-dependent positive feedback loop. Cell 2011;146:992–1003
53. Milbank E, Martinez MC, Andriantsitohaina R. Extracellular vesicles: pharmacological modulators of the peripheral and central signals governing obesity. Pharmacol Ther 2016;157:65–83
54. Finan B, Yang B, Ottaway N, et al. Targeted estrogen delivery reverses the metabolic syndrome. Nat Med 2012;18:1847–1856
55. Finan B, Clemmensen C, Zhu Z, et al. Chemical hybridization of glucagon and thyroid hormone optimizes therapeutic impact for metabolic disease. Cell 2016;167:843–857.e14